

How unique is Plaskett’s star? A search for organized magnetic fields in short period, interacting or post-interaction massive binary systems[★]

Yaël Nazé^{1†}, Coralie Neiner², Jason Grunhut^{3,4}, Stefano Bagnulo⁵, Evelyne Alecian⁶, Gregor Rauw¹, Gregg A. Wade⁷, and the BinaMIcS collaboration

¹ *Groupe d’Astrophysique des Hautes Energies - STAR, Institut d’Astrophysique et de Géophysique - B5c, Université de Liège, 19c Allée du 6 Août, B-4000 Sart Tilman, Belgium*

² *LESIA, Observatoire de Paris, PSL Research University, CNRS, Sorbonne Universités, UPMC Univ. Paris 06, Univ. Paris Diderot, Sorbonne Paris Cité, 5 place Jules Janssen, 92195 Meudon, France*

³ *European Southern Observatory (ESO), Karl Schwarzschild Strasse, 85 748, Garching bei München, Germany*

⁴ *Dunlap Institute for Astronomy and Astrophysics, University of Toronto, Rm 101, 50 St. George Street, Toronto, ON, M5S 3H4, Canada*

⁵ *Armagh Observatory and Planetarium, College Hill, Armagh, BT61 9DG, UK*

⁶ *Université Grenoble Alpes, IPAG, CNRS, 38000 Grenoble, France*

⁷ *Dept. of Physics, Royal Military College of Canada, P.O. Box 17000, Station Forces, Kingston, ON, Canada, K7K 4B4*

6 April 2024

ABSTRACT

Amongst O-type stars with detected magnetic fields, the fast rotator in the close binary called Plaskett’s star shows a variety of unusual properties. Since strong binary interactions are believed to have occurred in this system, one may wonder about their potential role in generating magnetic fields. Stokes *V* spectra collected with the low-resolution FORS2 and high-resolution ESPaDOnS and Narval spectropolarimeters were therefore used to search for magnetic fields in 15 interacting or post-interaction massive binaries. No magnetic field was detected in any of them, with 0 G always being within 2σ of the derived values. For 17 out of 25 stars in the systems observed at high-resolution, the 90% upper limit on the individual dipolar fields is below the dipolar field strength of Plaskett’s secondary; a similar result is found for five out of six systems observed at low resolution. If our sample is considered to form a group of stars sharing similar magnetic properties, a global statistical analysis results in a stringent upper limit of ~ 200 G on the dipolar field strength. Moreover, the magnetic incidence rate in the full sample of interacting or post-interaction systems (our targets + Plaskett’s star) is compatible with that measured from large surveys, showing that they are not significantly different from the general O-star population. These results suggest that binary interactions play no systematic role in the magnetism of such massive systems.

Key words: stars: early-type – stars: magnetic field – stars: individual: Plaskett’s star, HD1337, HD25638, HD35652, HD35921, HD57060, HD100213, HD106871, HD115071, HD149404, HD152248, HD190967, HD209481, HD228854, LSS3074, XZ Cep

1 INTRODUCTION

Prior to the early 2000s, no direct detection of magnetic fields in O-type stars had been reported. However, such fields

were strongly suspected to exist based on several indirect pieces of evidence, such as the presence of strong magnetic fields in the remnants of massive stars (pulsars and magnetars), of synchrotron radio emission in some massive binaries (for a review on non-thermal emitters, see Benaglia 2010), or of particular phenomena such as periodic modulations of line profiles (as e.g. in θ^1 Ori C, Stahl et al. 1996). Direct evidence of magnetism was finally acquired in the beginning of the 21st century. θ^1 Ori C was the first O-type star found to

[★] Based on observations collected at the European Organisation for Astronomical Research in the Southern Hemisphere under ESO programme 095.D-0075.

[†] FNRS Research Associate, E-mail: naze@astro.ulg.ac.be

be magnetic (Donati et al. 2002), HD 191612, an Of?p star, was the second (Donati et al. 2006), and many more have followed since then. Currently, about a dozen O-stars and several tens of early B-stars are known to be magnetic (see e.g. a summary by Petit et al. 2013), leading to an inferred incidence rate of such fields of about 6–8% amongst massive stars (Fossati et al. 2015b; Grunhut et al. 2016).

Some of the first detections were made in binaries: for example, θ^1 Ori C and HD 191612 are known to have companions. However, the orbital periods of these systems are long, implying that the binarity has little influence on the stellar properties. The case of Plaskett’s star is very different: this “star” actually is a binary system harbouring two late-type O-stars in a rather tight orbit with a period of 14.4 d (as first demonstrated by Plaskett 1922). It displays several peculiarities. The secondary star appears slightly more massive than the primary and rotates more than four times faster than its companion (Bagnuolo et al. 1992; Linder et al. 2008). The stars were classified O7.5I+O6I by Bagnuolo et al. (1992) and O8 III/I+O7.5 III by Linder et al. (2008) – but the latter authors noted that the secondary may actually be a O7V star that shows an apparent O7.5III spectrum because of its rapid rotation. A mismatch then exists between the spectroscopic masses and the dynamical ones, the latter being too large (Linder et al. 2008; Grunhut et al. 2013). Analyzing the optical spectra with atmosphere models further revealed that both stars are enriched in helium, that the secondary surface is depleted in nitrogen, and that the nitrogen abundance of the primary star is about 16 times that of the Sun while its carbon abundance is depleted by a factor of five (Linder et al. 2008, the N enrichment was already detected in X-ray data by Linder et al. 2006). In order to explain the unusual properties of the components, Bagnuolo et al. (1992) and Linder et al. (2008) proposed that the system is a post mass transfer binary in which the (currently) rapidly rotating secondary star received mass and angular momentum from its companion. In parallel, the Doppler maps derived from a tomographic analysis of the H α and He II λ 4686 lines revealed an annular emission region which was interpreted in terms of a flattening of the secondary’s wind (Linder et al. 2008). This was subsequently understood as a region of magnetically confined winds when a strong magnetic field was detected on this star ($B_d > 2.85$ kG, Grunhut et al. 2013). It is worth noting that Plaskett’s secondary is the only known rapidly-rotating magnetic O-star, hence the only O-star to appear in the centrifugally-supported magnetosphere zone of the confinement-rotation diagram (Petit et al. 2013).

The peculiar properties and evolutionary history of this system lead to speculations regarding the origin of the magnetic field of Plaskett’s secondary, with two main possibilities. On one hand, Plaskett’s secondary is a massive star, and global (i.e. not localized) magnetic fields in massive stars are generally thought to be fossil (e.g. Moss 2001, for a review see Neiner et al. 2015b and references therein). This could be the case of Plaskett’s secondary and, in this case, it would simply be amongst the few percent of magnetic objects in the massive star population. Its peculiarities – linked to binary interactions (stellar tides, see Palate & Rauw 2014, and previous mass transfer event, Linder et al. 2008) – would then be a coincidence. On the other hand, binarity could have played a key role, being di-

rectly responsible for the generation of a global magnetic field. This could occur through the triggering of differential rotation (e.g. Spruit 2002; Braithwaite 2006). Such a scenario was proposed by several authors, in particular to explain magnetism in massive stars as a result of stellar mergers (Ferrario et al. 2009; Langer 2014). Magnetism acquired after a merging event would naturally concern (currently) single magnetic objects or magnetic stars in long-period systems, but this idea cannot be applied directly to Plaskett’s star as it is a short-period system. However, “almost-merging” systems, after a common-envelope phase or a mass-transfer episode, should also experience strong shear, though discussions arose on whether such processes would also constitute a viable road towards magnetism. Indeed, some Be stars in binary systems may be the products of a past mass-transfer (van Bever & Vanbeveren 1997; McSwain & Gies 2005; de Mink et al. 2013, and references therein) but no large-scale magnetic field was detected for those objects (see Wade et al. 2016b and Sect. 3.3 of Rivinius et al. 2013, and references therein). Nevertheless, Plaskett’s star clearly appears as a potential candidate for this scenario (e.g. Langer 2014; Schneider et al. 2016). If true, it would have important implications for understanding the general pathways leading to the production of magnetic fields in massive stars.

In this study we set out to directly assess the validity of this scenario, which has never before been done, by verifying the magnetic status of “twins” of Plaskett’s star, defined as short-period massive binaries that interact or have interacted in the recent past. If binary interactions, in particular mass transfer events, constitute a dominant process for the generation of magnetic fields of massive stars, then most (if not all) of these systems would possess a magnetic component. In that case, we would thus have identified a specific group of magnetic O-stars, the second such category after the group of Of?p stars which were all found to be magnetic since the pioneering detection of 2006 (HD 191612, Donati et al. 2006; Wade et al. 2011; HD 148937, Hubrig et al. 2008; Wade et al. 2012a; HD 108, Martins et al. 2010; NGC1624-2, Wade et al. 2012b; CPD –28°2561, Hubrig et al. 2012; Wade et al. 2015). On the contrary, if mass transfer events are not a source of strong, large-scale magnetic fields, then the magnetic incidence in these systems would not differ significantly from that found for large stellar samples (Fossati et al. 2015b; Grunhut et al. 2016). In this paper, we report the results of such a campaign. Sections 2 and 3 present the targets and the observations used in this study, respectively, while Sect. 4 provides the results and Sect. 5 reports our conclusions.

2 THE SAMPLE

The first step of the project was to select interacting or post-interaction massive binaries. The key features to identify such systems are the sizes of the stars (e.g. filling their Roche lobes or close to doing so), but also the detection of non-solar abundances and/or of rotational asynchronicity, as well as a mismatch between predictions from evolutionary models of isolated stars and the observed stellar properties (age, masses, abundances, and luminosities). In addition, these binaries need to be bright enough to be observ-

able with the current generation of spectropolarimeters, but they also ought to be well known, i.e. to have reliable physical parameters, so that there is no ambiguity on their evolutionary status. Gies (2003) provided lists of well-studied double-lined spectroscopic (SB2) binary systems located in the Galaxy and the Magellanic Clouds, among which he separately listed unevolved cases (his Table 1) and evolved cases (his Table 2), the latter ones being subdivided between systems before contact, in contact, and after mass transfer. Penny et al. (2008) also listed binaries in which one star fills its Roche lobe, complementing the list. Eliminating the complex high-multiplicity systems δ Ori and Cyg OB2 5, which could blur the picture, while adding HD 149404 and LSS 3074, two other post-Roche Lobe Overflow (RLOF) systems not listed in these references but whose interactions were recently analyzed (see details below), we ended up with 15 relatively bright targets:

- *HD1337=AO Cas* (O9.7III+O9.5V) consists of two stars in a circular orbit of 3.5 d period (Stickland 1997; Linder 2008). The analysis of the eclipses yields a semi-detached configuration, with a ‘hot spot’ on the secondary possibly corresponding to the impact of an accreting stream (Linder 2008). Furthermore, stellar masses and radii appear too small compared to typical values for massive stars of the same spectral types, reinforcing the mass-transfer scenario (Linder 2008).

- *HD25638=SZ Cam* (O9.5V-9IV+B0-0.5V) comprises an eclipsing, circular SB2 system with a period of 2.7 d (Gorda 2015, and references therein). The derived radius of the primary is too large for a main sequence star while the mass of the secondary is too small for its spectral type (Lorenz et al. 1998). Furthermore, the derived masses, luminosities, and temperatures could not be fitted by theoretical evolutionary tracks, ruling out an ‘interaction-free evolution’ (Harries et al. 1998; Lorenz et al. 1998; Tamajo et al. 2012).

- *HD35652=IU Aur* (O9.5V+B0.5IV-V) comprises an eclipsing, semi-detached binary with a circular orbit and a period of $P=1.8$ d (Harries et al. 1998; Özdemir et al. 2003, and references therein). The derived masses and gravities of the stars cannot be explained by the separate evolution of massive stars born at the same time, suggesting a past mass-transfer event (Harries et al. 1998, see in particular their Fig. 9).

- *HD35921=LY Aur* (O9III+O9.5III) is a circular binary with a period of 4.0 d (Stickland et al. 1994; Zhao et al. 2014, and references therein). The analysis of the eclipses suggests a semi-detached or slightly overcontact configuration (Li & Leung 1985; Drechsel et al. 1989; Mayer et al. 2013) and the derived masses appear slightly too low (Stickland et al. 1994; Mayer et al. 2013), favouring an evolutionary scenario where mass-transfer has occurred.

- *HD57060=29 CMa* (O8.5I+O9.7V) is a slightly eccentric binary with a period of 4.4 d (Bagnuolo et al. 1994; Stickland 1997; Linder 2008). The photometric eclipses suggest some interaction between the stars (from semi-detached to overcontact configuration, Bagnuolo et al. 1994; Linder 2008; Antokhina et al. 2011) and the anomalous luminosities also seem to indicate an on-going mass-transfer. Furthermore, a tomographic analysis of the $H\alpha$ and He II 4686 lines (Linder 2008) and discrepancies in the mass ratio determination (Antokhina et al. 2011) suggest a flattened, disk-like

secondary wind, similar to that found in Plaskett's star. Finally, a wind-wind collision is also present in the system (Linder 2008).

- *HD100213=TU Mus* (O7.5V+O9.5V) is a binary with $e = 0$ and $P = 1.4$ d (Linder et al. 2007; Penny et al. 2008). Mutual irradiation of the stars in this very short-period system leads to the observation of line strength variations along the orbit (Linder et al. 2007; Palate et al. 2013). The eclipses of the system indicate that the stars are in contact while the masses derived from the orbital solution are lower than expected from evolutionary models, suggesting a past episode of mass-transfer (Linder et al. 2007; Qian et al. 2007; Penny et al. 2008, and references therein).

- *HD106871=AB Cru* (O8V+B0.5:) appears as a semi-detached, eclipsing binary with a circular orbit and a period of 3.4 d (Lorenz et al. 1994). A consistent fit to the derived properties of the stars (effective temperatures, radii, masses, luminosities) cannot be found with evolutionary tracks considering the absence of interaction while anomalous hydrogen and helium abundances are detected, both facts suggesting the system to have undergone mass-transfer (Lorenz et al. 1994).

- *HD115071* (O9.5V+B0.2III) consists of a semi-detached binary with a circular orbit and a period of 2.7 d (Penny et al. 2002). The ellipsoidal variations of its lightcurve indicate that the secondary star fills its Roche lobe. The derived masses are smaller than expected, suggesting mass-transfer to have occurred in a very recent past (Penny et al. 2002, and references therein).

- *HD149404* (O7.5If+ON9.7I) is a non-eclipsing, detached binary with a circular orbit and a period of 9.8 d (Rauw et al. 2001; Thaller et al. 2001). Emission lines such as $H\alpha$ and He II 4686 display phase-locked variations indicating the presence of a wind-wind collision (Rauw et al. 2001; Thaller et al. 2001). In addition, the secondary star is of the ON type, i.e. it presents anomalous abundances which hint at a past interaction (Rauw et al. 2001; Thaller et al. 2001). A recent, more detailed study further reveals an asynchronous rotation of the two stars, a significant nitrogen overabundance of the secondary star, and peculiar positions of the stars in the HR diagram (Raucq et al. 2016). All of these properties clearly disagree with expectations of single star evolutionary models, yielding further support to the past mass-exchange scenario (Raucq et al. 2016).

- *HD152248* (O7.5III(f)+O7III(f)) is a slightly eccentric and eclipsing binary with a period of 5.8 d (Sana et al. 2001; Mayer et al. 2008). Phase-locked variations in $H\alpha$ and He II 4686 lines as well as in the X-ray emission arise from a wind-wind collision located between the two stars (Sana et al. 2001, 2004). The derived masses are lower than expected from evolutionary tracks and both components appear close to filling their Roche lobes, suggesting a past mass-transfer episode (Sana et al. 2001). Note that tidal effects are reinforced by a small, non-zero, eccentricity.

- *HD190967* (O9.5V+B1I-II) consists of an eclipsing binary in a semi-detached configuration and with a period of 6.5 d and $e = 0$ (Harries et al. 1997; Kumsiashvili et al. 2005). In a mass-gravity diagram, the derived values are at odds with predictions of evolutionary models for stars of the same age, indicating a past episode of rapid mass-transfer (Harries et al. 1997; Kumsiashvili et al. 2005). Note that, to best fit the lightcurve, either bright spots or an accretion

Table 1. Summary of the properties of our targets and of Plaskett’s star

ID	V	Sp. Types	P (d)	e	C/SD?	AA?	Mass gainer	$v\sin(i)$ (km s ⁻¹) prim-sec-tert
Plaskett’s star	6.06	O8III/I+O7.5III	14.4	0	N	Y	sec.	77-370*
HD 1337	6.14	O9.7III+O9.5V	3.5	0	Y		sec.	118-82*
HD 25638	6.93	O9.5V-9IV+B0-0.5+B0III-III	2.7	0	N		prim.	137-69-40*
HD 35652	8.39	O9.5V+B0.5IV-V+B	1.8	0	Y		prim.	172-159-71*
HD 35921	6.85	O9III+O9.5III+B	4.0	0	Y		prim.?	202-122-27*
HD 57060	4.95	O8.5I+O9.7V	4.4	0.1	Y		sec.	107-193*
HD 100213	8.41	O7.5V+O9.5V	1.4	0	Y			222-191
HD 106871	8.48	O8V+B0.5:	3.4	0	Y	Y	prim.	
HD 115071	7.97	O9.5V+B0.2III	2.7	0	Y		prim.	101-132
HD 149404	5.47	O7.5If+ON9.7I	9.8	0	N	Y	prim.	56-80*
HD 152248	6.05	O7.5III(f)+O7III(f)	5.8	0.1	N			139-128*
HD 190967	8.16	O9.5V+B1I-II	6.5	0	Y		prim.	230-115*
HD 209481	5.55	O9III+ON9.7V	3.1	0	N	Y	prim.	127-93*
HD 228854	8.65	O7.3V+O7.7V	1.9	0	Y			223-203*
LSS 3074	11.7	O4If+O7.5	2.2	0	N	Y	sec.	110-127
XZ Cep	8.51	O9.5V+B1III	5.1	0	Y		prim.	104-172*

Evidence for current or past interaction (for references, see text): “C/SD” = in a contact or semi-detached configuration, “AA” = abundances anomalies detected - note that there are also other anomalies detected (e.g. too low masses, asynchronous rotation,...), see text for details. The projected rotational velocities $v\sin(i)$ are given for primary and then secondary then tertiary, they come from our analysis of high-resolution spectra when an asterisk is added and from literature otherwise (Howarth et al. 1997 for HD 100213, otherwise see dedicated items in text for literature references).

disk are needed (Kumsiashvili et al. 2005; Djurašević et al. 2009).

- *HD209481=LZ Cep* (O9III+ON9.7V) is a binary with a circular orbit and a period of 3.1 d. The ellipsoidal variations of its optical lightcurve indicate that both stars almost fill their Roche lobes (Mahy et al. 2011; Palate et al. 2013). Several lines of evidence point towards a past mass-transfer episode (Harries et al. 1998; Mahy et al. 2011): the photosphere of the secondary star appears strongly enriched in helium and nitrogen but depleted in carbon and oxygen, there is a slight asynchronicity between the rotation periods, and the evolutionary masses are higher than the masses inferred from the orbital solution.

- *HD228854* (O7.3V+O7.7V) is a system with a circular orbit and a period of 1.9 d (Yaşarsoy & Yakut 2013, and references therein). The analysis of the eclipses indicates filling of the Roche lobe(s) (either overcontact, Degirmenci et al. 1999; Qian et al. 2007, or contact/semi-detached, Mayer et al. 2002; Yaşarsoy & Yakut 2013) and the derived physical properties (in particular masses and gravities) disagree with theoretical expectations for (single) massive star evolution (Harries et al. 1997), pointing towards a post mass-transfer situation.

- *LSS3074* (O4If+O7.5f) is a circular binary with a period of 2.2 d (Niemela et al. 1992; Haefner et al. 1994, and Raucq et al. 2017 submitted). $H\alpha$ and $He\text{II}4686$ lines present line profile modulations that are reminiscent of those observed in HD 149404, suggesting wind-wind collision to be present (Raucq et al., 2017, submitted). Photometric, spectroscopic, and polarization measurements led to the derivation of the physical parameters for the system (Niemela et al. 1992, and Raucq et al. 2017 submitted). The anomalous abundances as well as the mismatch between evolutionary tracks and observed masses and luminosities suggest a mass-transfer in the system (Raucq et al. 2017 submitted).

- *XZ Cep* (O9.5V+B1III) is a non-eccentric, eclipsing system with a period of 5.1 d (Harries et al. 1997). The sec-

ondary star fills its Roche lobe while the derived stellar properties are at odds with predictions from evolutionary models (incompatible ages for the derived masses and gravities, Harries et al. 1997), suggesting a previous episode of mass-transfer.

Evidence for past or current interactions (abundance anomalies, Roche lobe filling,...) in the chosen systems has just been mentioned above (see Table 1 for a summary), but the presence of such interactions does not necessarily imply that they were actually efficient in modifying the stellar structure. In particular, Plaskett’s secondary displays a high rotation rate (~ 300 km s⁻¹, Bagnuolo et al. 1992; Linder et al. 2008; Grunhut et al. 2013), demonstrating that momentum exchange was very efficient for that object. For the stars in our sample, projected rotational velocities are also rather high and generally amount to 100–200 km s⁻¹, with components in four systems (HD 35921, HD 100213, HD 190967, and HD 228854) reaching even higher velocities ($v\sin(i) > 200$ km s⁻¹ see Table 1). This confirms that our sample is well suited to find out whether magnetic fields are triggered in massive binary interactions.

3 OBSERVATIONS

For the Northern targets, high-resolution spectropolarimetry was acquired with ESPaDOnS at CFHT (Donati 2003) and Narval at TBL (Aurière 2003). For the Southern targets, low-resolution spectropolarimetry was acquired with FORS2 at ESO (Appenzeller & Rupprecht 1992; Szeifert et al. 1998). Two targets, HD 152248 and HD 149404, were observed at both low and high resolutions, as they are visible from Chile as well as from Hawaii.

3.1 Low-resolution FORS2 spectropolarimetry

Low-resolution spectropolarimetric data of six targets were obtained with the Very Large Telescope equipped with FORS2 in Spring 2015 (ESO 095.D-0075, PI Nazé, see Table 2). These data were taken in service mode with the red CCD (a mosaic composed of two 2k×4k MIT chips), no binning, a slit of 1" and the 1200B grating ($R \sim 1400$). The observing sequence consisted of 8 subexposures with retarder waveplate positions of $+45^\circ$, -45° , -45° , $+45^\circ$, $+45^\circ$, -45° , -45° , $+45^\circ$. We reduced these spectropolarimetric data with IRAF as explained by Nazé et al. (2012): the aperture extraction radius was fixed to 20 pixels, the nearby sky background was subtracted, and wavelength calibration was performed from 3675 to 5128Å (with pixels of 0.25Å) considering arc lamp data taken at only one retarder waveplate position (in our case, -45°). There was no indication of variation of the Stokes I spectra between subexposures. We then constructed the normalized Stokes V/I profile, as well as a diagnostic "null" profile N/I (see Donati et al. 1997; Bagnulo et al. 2009, for details on the procedure and Fig. 1 for an illustration in our case). Finally, the associated longitudinal magnetic field was estimated by minimizing $\chi^2 = \sum_i \frac{(y_i - B_z x_i - a)^2}{\sigma_i^2}$ with y_i either V/I or the null profile at the wavelength λ_i and $x_i = -g_{\text{eff}} 4.67 \times 10^{-13} \lambda_i^2 1/I_i (dI/d\lambda)_i$ (Bagnulo et al. 2002). This was done for x_i in the interval between -10^{-6} and $+10^{-6}$, after discarding edges and deviant points and after selecting spectral windows centered on stellar lines (see Nazé et al. 2012, for further discussion). These windows comprise both primary and secondary absorption lines, but avoid emission lines (as some of them arise in wind-wind collision regions and are thus not representative of the stellar photosphere). The values reported in Table 2 were obtained after rectifying the Stokes profiles, but similar values are found if no rectification is applied.

3.2 High-resolution ESPaDOnS and Narval spectropolarimetry

Most high-resolution spectropolarimetric data of our targets were collected in the context of the MiMeS (Wade et al. 2016a) and the BinaMicS (Alecian et al. 2015) large programmes. They were acquired with ESPaDOnS, an echelle spectropolarimeter installed at the Canada-France-Hawaii Telescope. In addition, archival data from dedicated programmes (PIs Neiner, Bouret) were obtained for HD 209481 in 2006 and 2009 using Narval, a similar spectropolarimeter installed at Pic du Midi (France). Biases, flat-fields, and ThAr calibrations were obtained at the beginning and at the end of each night. The data reduction was performed using Libre-Esprit, the dedicated reduction software based on Esprit (Donati et al. 1997). There was no indication of variation of the Stokes I spectra between subexposures. Normalization of the individual orders was then performed using low-degree polynomial fits.

After the Stokes spectra were calculated, we followed the same procedure as Grunhut et al. (2016). First, the Least-Squares Deconvolution technique (LSD, Donati et al. 1997; Kochukhov et al. 2010) was applied to all polarimetric spectra to increase the signal-to-noise, thereby helping to detect weak magnetic Zeeman signatures (see Fig. 2 for

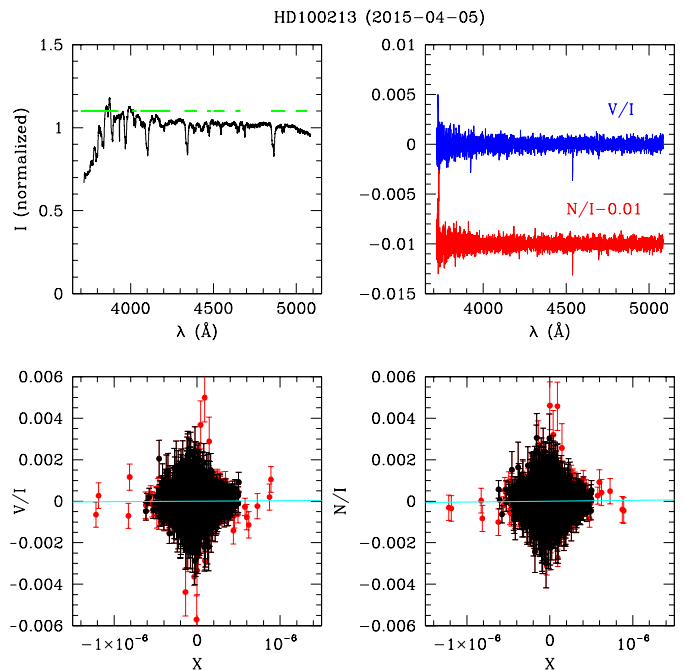


Figure 1. *Top Left:* The spectrum of HD 100213 taken on the second night of observation with FORS2, with the selected windows shown by a green thick line. *Top right:* Associated V/I (top blue) and N/I (bottom red) as a function of wavelength. *Bottom:* V/I (left) and N/I (right) as a function of x_i , with their best-fit straight lines shown in cyan. Rejected values, not considered for the fitting, appear in red. Note the null slopes of the best-fit straight lines, that indicate the absence of a significant magnetic field.

an illustration). We first constructed a line mask from the VALD2 database (Piskunov et al. 1995; Kupka et al. 1999) using the appropriate temperature and $\log(g)$ values for each star, assuming solar abundances and considering only lines deeper than 1% of the continuum. We then excluded all hydrogen lines and lines blended with hydrogen. This yielded masks with between 430 and 1220 lines, depending on the star, over the 3700–9800Å interval. The line depths were then adjusted to provide the best fit to the observed Stokes I spectrum of each target. Note that regularisation (see Kochukhov et al. 2010) and clipping of the deviant points were both applied to improve the final signal-to-noise of the LSD profiles.

Since our targets are binaries, the second step was to derive the individual properties of each component (see Fig. 2 and Grunhut et al. 2016 for details on the procedure). To this aim, multiple absorption components with profiles derived from the convolution of a rotationally broadened profile with a radial-tangential macroturbulence profile were fitted to the Stokes I profiles. Since this disentangling process often leads to degenerate solutions, relevant information (e.g. $v \sin(i)$) from the literature was used to constrain the fits, whenever needed. The derived RVs were checked for compatibility with the known orbital solutions of these systems, i.e. we verified that each observed pair of RVs agreed with the solution at *some* phase during the orbit (accurate orbital phases at current epoch cannot be computed due to

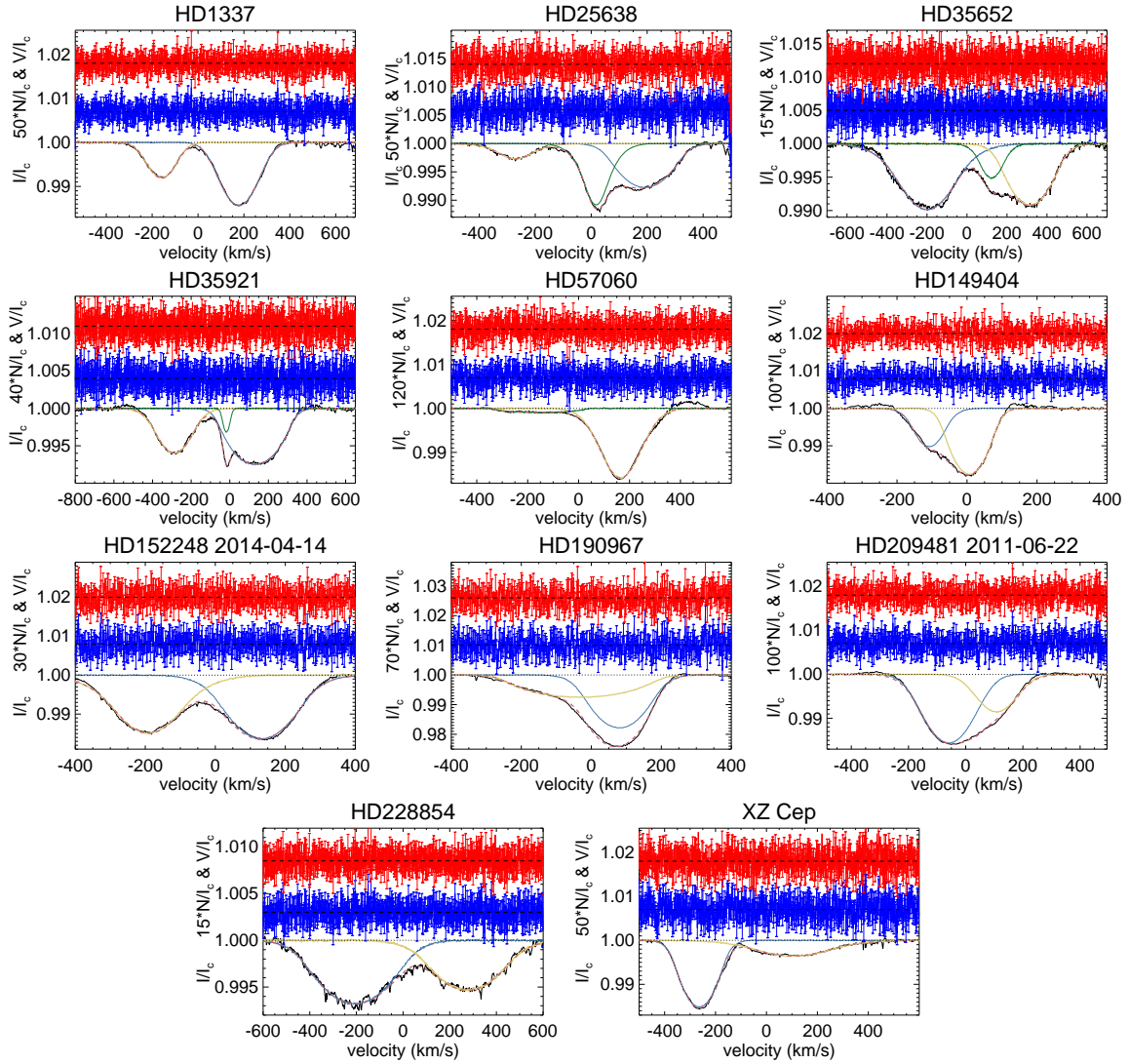


Figure 2. LSD profiles derived for the BinaMiCS sample (coming from [Grunhut et al. 2016](#) for the three MiMeS targets - HD 1337, HD 35921, HD 209481). Each panel provides, from top to bottom, the system name and the Stokes V , N , and I profiles, respectively. The individual components of the I profiles, derived from the disentangling procedure described in Sect. 3.2, are added with colours (yellow, blue, or green solid lines) along with their sum (dashed red lines).

Table 2. Results from the low-resolution spectropolarimetry obtained with FORS2.

ID	L_1/L_2	Exp. (s)	SNR	Date	HJD-2450000.	B_z (G)	N_z (G)
HD 100213	~ 2	8×70	2470	2015-04-03	7115.687	34±48	2±47
		8×70	2365	2015-04-05	7117.732	24±50	37±49
HD 106871	~ 2.5	8×80	2210	2015-04-03	7115.733	-31±45	3±44
		8×80	2380	2015-04-05	7117.754	32±39	60±38
HD 115071	~ 0.9	8×60	2350	2015-04-05	7117.837	-22±34	-44±33
		8×60	2520	2015-05-01	7143.618	-42±32	16±33
HD 149404	~ 0.7	8×7	1650	2015-05-16	7158.907	214±119	-234±117
		8×7	2130	2015-05-17	7159.585	-64±80	3±69
HD 152248	0.8–1.	8×10	2100	2015-05-02	7144.620	-25±69	36±63
		8×10	1845	2015-05-17	7159.570	29±59	90±59
LSS 3074	1.–2.5	8×536	1400	2015-04-03	7115.809	-591±619	200±427
		8×536	1450	2015-04-05	7117.796	-452±391	187±362

From left to right, the columns show the binaries' names, the light ratios (see Sect. 2 for references), the exposure lengths, the peak signal-to-noise ratio in the 4000–5000Å range, the observing times (both in YYYY-MM-DD format and in heliocentric Julian dates), and finally the derived magnetic field values and their associated errors for both the system's Stokes V profile and from the null diagnostic profile. These B_z and N_z values were found using rectification and within selected spectral windows.

the large accumulated phase uncertainties). Disentangled I profiles were then obtained for each system component, and used to estimate individual V and N contributions. Note that, if line profiles overlap and one component is magnetic, this procedure does not account for the possible magnetic contamination caused by the Stokes V signal of the companion.

Finally, the magnetic properties were derived from the Stokes V profiles. We calculated in each case the probability that deviations of the observed V/I_c signal from the normalized value of 0 occur by chance (i.e. because of noise only - see Donati et al. 1992, but note that this reference reports the complement probability). This was done using an optimal velocity grid (with a minimum resolution of 1.8 km s^{-1}) representing the best compromise between increasing the signal-to-noise and not smearing the Zeeman signature. Next, the longitudinal field values B_z were computed from the first-order moment of the unbinned Stokes V profiles (Mathys 1989; Donati et al. 1997), with errors derived by propagating the known uncertainties for each pixel. Similar measurements were made for the diagnostic null profiles N . Note that the field values for the MiMeS targets (HD 1337, HD 35921, and HD 209481) were already reported by Grunhut et al. (2016).

Since the significance level (or false-alarm probability) was larger than 10^{-3} in each case, corresponding to clear non-detections, upper limits on the dipolar field values were derived using Monte-Carlo simulations as described by Neiner et al. (2015a) and Blazère et al. (2015). For both the primary and secondary, we simulated 1000 oblique dipole models for various values of the polar magnetic field strength with random inclination angles i , obliquity angles β , and rotational phases. White Gaussian noise with a null average and a variance corresponding to the signal-to-noise of each observed profile was added. Using the best-fit disentangled LSD I profiles, we calculated local Stokes V profiles assuming the weak-field case, which were then integrated over the visible hemisphere of the star. The derived synthetic Stokes V profiles were normalized to the intensity of the continuum, and the Neyman-Pearson likelihood ratio test was then applied to estimate the probability of detecting a dipolar oblique magnetic field (with a threshold of 10^{-3} for the false alarm probability). A 90% detection rate was required to consider that the simulated field would statistically be detected in the data. This translates into upper limits for the possible undetected dipolar field strength for each star and each observation. For HD 152248 and HD 209481, multiple observations were available and since none of them resulted in a magnetic detection, single-observation statistics were combined to extract a stricter upper limit on the non-detected field (see Sect. 4.2 of Neiner et al. 2015a for details).

4 RESULTS AND DISCUSSION

Table 2 reports the resulting longitudinal magnetic field values¹ for the low-resolution spectropolarimetric data, while

¹ They are weighted averages of the contributions of all components in each system, i.e. each value is valid for the entire system. The light ratios L_1/L_2 of the systems are known (Table 2).

Table 3 provides the field values derived from each high-resolution spectropolarimetric observation for individual components and for each system as well as upper limits on non-detected magnetic fields per component from individual and combined observations. It is clear from these tables (see also Fig. 3) that (1) no problem due to spurious signals affects the data (the null diagnostics being always compatible with zero within 2σ at most - and generally well within 1σ) and (2) no significant magnetic field is detected for any of the systems or their components.

One caveat must however be mentioned: when using low-resolution spectropolarimeters like FORS2, even strong fields may become unobservable, depending on the magnetic geometry of the star and the observing phase. Indeed, as the sinusoidal B_z curve of magnetic oblique rotators reaches or nears a value of 0 G at cross-over phases (i.e. when the dipole is seen equator-on), the field would become undetectable in low resolution observations. However, this occurs during a small fraction of the rotational period only, an interval depending on the error bars. For example, we may consider Plaskett's B_z values (Grunhut et al. 2013) and assume a sinusoidal B_z varying from -810 G to 680 G. Non-detections imply $B_z \sim 0$, i.e. $|B_z| < N\sigma$ with N generally taken to be 3 (though a value of 5 appears better suited for FORS, see Bagnulo et al. 2002). Since the typical error on the ten FORS measurements amounts to ~ 55 G, excluding the more uncertain case of LSS 3074, non-detections would then occur during 15% of the orbit if we consider 3σ , or 25% for a 5σ threshold. Missing a detection is less probable when several observations of the same target are acquired, as was done for all systems observed at low resolution. Indeed, it is unlikely to have two random exposures sampling cross-over phases for one target. Moreover, if it is already unlikely for one target, it is even more so for several independent objects. Considering a 15% chance to miss detecting a Plaskett-like field in one observation, the probability to miss field detections in *all* ten observations is $(0.15)^{10} \sim 10^{-8}$ (or 10^{-6} if 25% is considered). Of course, there is a high chance ($\sim 80\%$) to miss one detection over ten observations, but since we have two observations of each target and two targets in common with the high-resolution sample, then this risk may be mitigated. One could object that some of the observation pairs are separated by only one or two days, so that there would be no large phase change over that interval if the rotational period is long. However, it must be remembered that, contrary to the "usual" magnetic massive stars, our targets are relatively fast rotators in short-period systems so that B_z should change rapidly, with significant variations expected on the timescale of one day, as observed for Plaskett's star. Moreover, even if we do consider that the two observations of a target were taken at the same rotational phase, the probability to miss a field in all five cases is still low: $(0.15)^5 \sim 10^{-4}$ considering a 15% chance of missing the field detection, or 10^{-3} if a 25% chance is used instead. Therefore, statistically, we could have missed detecting the magnetic field of

However, deriving individual limits from the system's values is not straightforward, since longitudinal fields are derived from the analysis of sets of lines, whose strengths for primary and secondary do not necessarily reflect the light ratios between components and furthermore vary with ion under consideration. We therefore refrain from deriving individual limits.

Table 3. Results from the high-resolution ESPaDOnS and Narval spectropolarimetry.

ID	Exp. /SNR	Date	HJD -2.45e6	Obj	V_r (km s ⁻¹)	B_z (G)	N_z (G)	σ (G)	up. lim. (kG)
HD 1337	4×720 1280	2009-10-09	5113.845	prim	178	46	-37	39	1.0
				sec	-160	-46	-134	74	1.9
				system		35	40	60	
HD 25638	8×840 1557	2013-11-20	6616.786	prim	193	-62	-7	69	1.7
				sec	-272	-112	-154	241	6.8
				tert	17	-12	-62	55	2.0
HD 35652	8×840 942	2016-02-27	7445.812	system		-55	85	101	
				prim	-198	-122	-42	267	7.1
				sec	315	216	120	205	4.8
HD 35921	4×940 1215	2011-11-13	5878.872	tert	124	189	-368	329	8.7
				system		37	-161	249	
				prim	130	-102	-44	75	1.7
HD 57060	12×540 2942	2013-03-03	6354.835	sec	-287	76	-48	104	2.8
				tert	-18	16	-45	74	2.0
				system		74	-15	98	
HD 149404	16×390 3038	2014-06-08	6816.897	prim	160	17	-5	15	0.6
				sec	-141	173	286	196	3.3
				system		92	102	47	
HD 152248	4×540 794	2014-04-13	6761.045	prim	-108	14	-10	25	0.7
				sec	7	34	4	16	0.3
				system		35	9	16	
HD 152248	12×540 1358	2014-04-14	6762.060	prim	-135	-175	-72	155	4.1, <i>comb: 1.5</i>
				sec	111	416	-148	206	5.4, <i>comb: 1.9</i>
				system		-9	-39	148	
HD 190967	8×840 989	2016-05-18	7527.097	prim	129	112	88	89	2.2
				sec	-192	-153	-135	104	2.5
				system		-46	7	97	
HD 209481	4×600 867	2006-12-14	4084.274	prim	-32	-15	-15	87	2.1
				sec	80	-3	21	32	0.9
				system		-14	-13	46	
HD 209481	4×675 667	2009-07-20	5033.483	prim	74	14	60	74	1.7, <i>comb: 0.4</i>
				sec	-226	-36	51	120	3.1, <i>comb: 0.6</i>
				system		-34	107	91	
HD 209481	4×675 667	2009-07-20	5033.483	prim	27	-73	124	97	2.3
				sec	-100	160	-168	134	3.4
				system		-46	-10	65	
HD 209481	4×825 1191	2009-07-24	5037.485	prim	-98	85	-32	48	1.1
				sec	212	213	24	83	2.1
				system		99	-87	63	
HD 209481	4×675 916	2009-07-25	5038.492	prim	26	59	2	66	1.5
				sec	-95	-51	60	107	2.7
				system		-34	33	45	
HD 209481	4×675 804	2009-07-26	5039.492	prim	46	192	67	62	1.4
				sec	-154	-225	9	90	2.3
				system		16	0	54	
HD 209481	4×675 315	2009-07-27	5040.490	prim	-97	142	-112	180	4.2
				sec	212	-459	-307	322	8.3
				system		-12	-80	238	
HD 209481	4×675 1058	2009-07-28	5041.480	prim	10	26	-9	54	1.2
				sec	-66	5	1	76	1.9
				system		-19	-2	29	
HD 209481	4×675 1199	2009-07-29	5042.496	prim	54	23	-62	48	1.1
				sec	-174	-21	128	70	1.8
				system		26	-19	46	
HD 209481	4×675 1037	2009-07-30	5043.476	prim	-96	85	-17	60	1.4
				sec	201	-62	-49	100	2.5
				system		76	25	69	
HD 209481	4×675 1105	2009-07-31	5044.496	prim	-4	2	-39	57	1.3
				sec	-40	40	-17	86	2.2
				system		-19	-32	30	

Table 3. Continued.

ID	Exp. /SNR	Date	HJD -2.45e6	Obj	V_r (km s ⁻¹)	B_z (G)	N_z (G)	σ (G)	up. lim. (kG)
HD 209481	4×675 968	2009-08-03	5047.461	prim	-24	39	-69	69	1.6
				sec	6	71	5	89	2.2
				system		46	-2	32	
HD 209481	12×400 2417	2011-06-22	5735.027	prim	-60	3	2	22	0.5
				sec	108	-3	-6	39	1.0
				system		1	-16	17	
HD 228854	8×840 975	2016-05-17	7526.067	prim	-206	-142	-146	188	5.7
				sec	275	-122	142	256	7.6
				system		27	208	269	
XZ Cep	8×840 609	2013-08-19	6523.930	prim	-265	-30	5	45	1.1
				sec	103	621	-473	488	11.1
				system		37	-180	184	

From left to right, the columns provide the binaries’ names, the exposure lengths and peak signal-to-noise ratios in the 5000–6500 Å range, the observing times (both in YYYY-MM-DD format and in heliocentric Julian dates), the considered component, its heliocentric velocity, the magnetic field values and their associated errors (σ) derived from the system’s Stokes V profile (B_z) and from the null diagnostics profiles (N_z), and finally the upper limits on the dipolar field strength with 90% chance of being detected. When several observations of the same target are available (as for HD 152248 and HD 209481), the upper limit on the undetected field from the combined statistics is quoted in italics in the last column of the first observation line after a “comb” prefix.

one star in the FORS2 sample, but not more. Note that for high-resolution data, this problem does not exist as a single random observation has proven to be efficient to detect magnetism (when it exists) in a massive star during the MiMeS, BinaMIcS, and other magnetic surveys (see also a more theoretical discussion by [Petit & Wade 2012](#)). Indeed, except in very rare cases², even if the derived longitudinal field is zero, the high-resolution Stokes V profile of a magnetic object is not flat and the field can be detected whatever the phase. Missing the detection of a strong field in the high-resolution sample thus is unlikely.

It is important to note that the error bars on B_z are small (σ smaller than 100 G), except for a few cases - for FORS data, only LSS 3074 has large error bars ($\sigma > 100$ G) because it is a faint object ($B \sim 13$ mag compared to $B = 5 - 9$ for the others); for ESPaDOnS/Narval data, large errors are only found for all components of HD 35652 and HD 228854, as well as the secondary stars of HD 25638, HD 57060, and XZ Cep. Hence our survey is generally very sensitive. In the high-resolution data, this is also reflected by the determination of the upper limits on the dipolar fields which could have remained hidden in the noise for each target. The limits are well below the field strength of Plaskett’s star ($B_d > 2.85$ kG, [Grunhut et al. 2013](#)) for the vast majority of the cases (17 out of 25 limits on individual components).

The objective of this paper is to test the plausibility of binary interactions as efficient processes at generating stable magnetic fields in massive systems. If this were true, we would expect all our targets to share similar properties, different from the usual massive star population. In such a case, we can further statistically characterize our sample

by following the Bayesian approach of [Kolenberg & Bagnulo \(2009\)](#), see in particular their Eq. (7), later generalised by [Asensio Ramos et al. 2015](#)). It assumes that all stars of our sample are similar, i.e. they have a dipolar field with identical field strength, but their magnetic axes are randomly oriented with respect to the line-of-sight, and it combines the observational values into a constraint on the common field strength. We note that Eq. (7) of [Kolenberg & Bagnulo \(2009\)](#) is valid only for independent measurements on different stars, therefore for those objects that have been observed more than once we have considered only the field measurement with the smallest error bar. Note also that Eq. (7) has been applied twice (see Fig. 3): first to measurements of individual stars (results from high-resolution data for stars labelled “primary”, “secondary”, or “tertiary” in Table 3), second to field estimates for the systems (combining results from Table 2 for low-resolution observations and those listed under the “system” label in Table 3 for high-resolution observations). We then derive that there is a 90% chance that the dipolar field strength at the pole is $B_d \leq 140 - 220$ G, a very stringent limit well below Plaskett’s secondary field. Hence our sample and Plaskett’s star, while having all underwent binary interactions, do not seem to form a specific and coherent group of magnetic stars.

To shed more light onto our results, we can compare them to the current knowledge of large-scale magnetic fields in massive stars. Such fields are generally considered to be (mostly) dipolar. In addition, except for ζ Ori A (a supergiant O-star with an extremely low field, [Blazère et al. 2015](#)) and β CMa ([Fossati et al. 2015a](#)), the detected fields are strong, with B_d larger than 0.5 kG for O and B0.5–1 stars (e.g. [Petit et al. 2013](#)). This is notably the case of Plaskett’s secondary. The detection rate of such fields, found in large samples composed of single massive stars and/or long-period massive binaries, amounts to 6–8% ([Fossati et al. 2015b](#); [Grunhut et al. 2016](#)). How does that compare to the case of massive interacting or post-interaction binaries? Overall, we have one magnetic detection (Plaskett’s star) in 16 investigated multiple systems (our sample + Plaskett’s star, comprising 35 individual stars in total). If we exclude the tar-

² When both components are magnetic, when the observation has been obtained at conjunction, and when the signatures of both components are of opposite shape and cancel each other either partially or totally, the magnetic signal could be diluted and not be detected if present. Note however that not only is this case very unlikely but none of our targets was observed at conjunction, as demonstrated by the very different velocities in Table 3 (see also Fig. 2 for a visual inspection of the components’ separations).

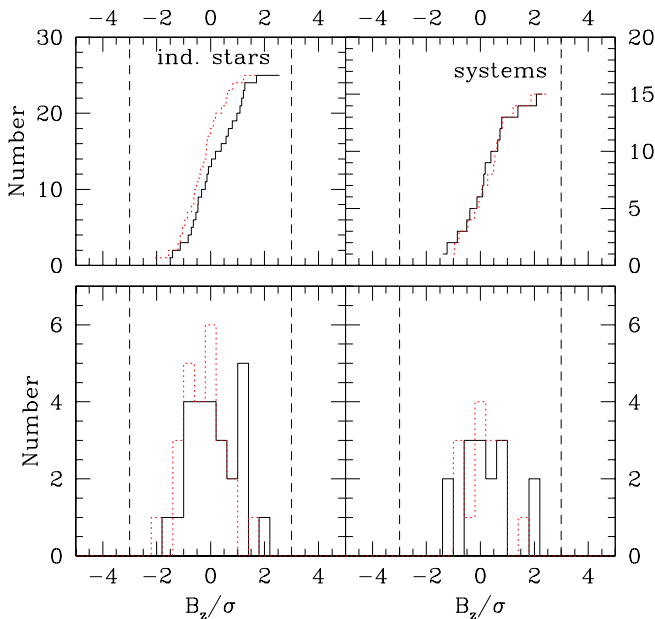


Figure 3. Cumulative (top) or simple (bottom) distribution of the B_z values normalized to their error bars for our sample (left, for B_z values of individual stars - labelled “primary”, “secondary”, or “tertiary” in Table 3; right, for B_z values estimated for the whole system - from Table 2 for FORS measurements and under “system” label in Table 3 for high-resolution observations). The dotted red lines are for the N_z values, while the dashed vertical lines correspond to a 3σ detection level. Note how the measured values are all within 2σ from zero.

gets with less stringent constraints, then the high-resolution data yield one magnetic detection (Plaskett’s secondary) on 19 stars. If we keep only *individual* measurements with field limits lower than Plaskett’s field (2.85 kG), one on 17 stars for a limit of 2 kG, and one on 9 stars for a limit of 1 kG. Focusing only on the mass gainers (Plaskett’s secondary + those of our sample - when known, see Table 1), there is one magnetic object out of 8 stars measured at high resolution with small error bars. In summary, whatever the case under consideration, these incidence levels appear entirely compatible with that derived from general samples, considering the small number statistics. The incidence rate in the interacting/post-interaction binary sample is thus *not* much larger than for the general O-star population. Therefore, there is no need to include additional processes linked to binary interactions to explain the presence of a magnetic field in Plaskett’s secondary.

5 CONCLUSION

Amongst magnetic O-stars, one object is particularly remarkable: the secondary of Plaskett’s star, a binary system which has very likely undergone mass-transfer in the recent past. This situation led to the intriguing possibility that binary interactions could be a source of magnetism in massive stars. To test the validity of this scenario, we have observed a

sample of 15 interacting and post-interaction systems. Dedicated spectropolarimetry did not lead to any magnetic detection in these systems. In fact, for the vast majority of our targets, the longitudinal fields are <300 G and the individual upper limits on the dipolar fields are below the dipolar field strength of Plaskett’s secondary for 17 out of 25 binary components. Considering our targets as an homogeneous group of similar objects, a global statistical analysis of the derived field values leads to a 90% upper limit on the (common) dipolar field strength of only 140–220 G, underlining once again the dissimilarity between our targets and Plaskett’s star. Moreover, the low rate of magnetic detection in these interacting and post-interaction systems is compatible with the rates found from general surveys of O-stars. Together with the lack of magnetic detection in Be stars, some of which are also likely products of mass-transfer, this suggests that binary interactions do not systematically trigger stable, strong magnetic fields in such systems, and that a fossil origin is still the best scenario for explaining the magnetic fields of massive stars.

ACKNOWLEDGEMENTS

YN and GR acknowledge support from the Fonds National de la Recherche Scientifique (Belgium), the Communauté Française de Belgique, the PRODEX XMM contract (Belspo), and an ARC grant for concerted research actions financed by the French community of Belgium (Wallonia-Brussels Federation). GAW acknowledges Discovery Grant support from the Natural Science and Engineering Research Council (NSERC) of Canada.

REFERENCES

- Alecian, E., Neiner, C., Wade, G. A., et al. 2015, *New Windows on Massive Stars*, 307, 330
- Antokhina, E. A., Srinivasa Rao, M., & Parthasarathy, M. 2011, *New Astron.*, 16, 177
- Appenzeller, I., & Rupprecht, G. 1992, *The Messenger*, 67, 18
- Asensio Ramos, A., Martínez González, M. J., & Manso Sainz, R. 2015, *A&A*, 577, A125
- Aurière, M. 2003, *EAS Publications Series*, 9, 105
- Bagnulo, S., Szeifert, T., Wade, G. A., Landstreet, J. D., & Mathys, G. 2002, *A&A*, 389, 191
- Bagnulo, S., Landolfi, M., Landstreet, J. D., et al. 2009, *PASP*, 121, 993
- Bagnuolo, W. G., Jr., Gies, D. R., & Wiggs, M. S. 1992, *ApJ*, 385, 708
- Bagnuolo, W. G., Jr., Gies, D. R., Hahula, M. E., Wiemker, R., & Wiggs, M. S. 1994, *ApJ*, 423, 446
- Benaglia, P. 2010, *High Energy Phenomena in Massive Stars*, 422, 111
- Blazère, A., Neiner, C., Tkachenko, A., Bouret, J.-C., & Rivinius, T. 2015, *A&A*, 582, A110
- Braithwaite, J. 2006, *A&A*, 449, 451
- Carrier, F., North, P., Udry, S., & Babel, J. 2002, *A&A*, 394, 151
- Değirmenci, Ö. L., Sezer, C., Demircan, O., et al. 1999, *A&AS*, 134, 327
- de Mink, S. E., Langer, N., Izzard, R. G., Sana, H., & de Koter, A. 2013, *ApJ*, 764, 166
- Djurašević, G., Vince, I., Khruzina, T. S., & Rovithis-Livaniou, E. 2009, *MNRAS*, 396, 1553
- Donati, J.-F. 2003, *Solar Polarization*, 307, 41

- Donati, J.-F., & Landstreet, J. D. 2009, *ARA&A*, 47, 333
- Donati, J.-F., Semel, M., & Rees, D. E. 1992, *A&A*, 265, 669
- Donati, J.-F., Semel, M., Carter, B. D., Rees, D. E., & Collier Cameron, A. 1997, *MNRAS*, 291, 658
- Donati, J.-F., Babel, J., Harries, T. J., et al. 2002, *MNRAS*, 333, 55
- Donati, J.-F., Howarth, I. D., Jardine, M. M., et al. 2006, *MNRAS*, 370, 629
- Drechsel, H., Lorenz, R., & Mayer, P. 1989, *A&A*, 221, 49
- Ferrario, L., Pringle, J. E., Tout, C. A., & Wickramasinghe, D. T. 2009, *MNRAS*, 400, L71
- Fossati, L., Castro, N., Morel, T., et al. 2015a, *A&A*, 574, A20
- Fossati, L., Castro, N., Schöller, M., et al. 2015b, *A&A*, 582, A45
- Gies, D. R. 2003, *A Massive Star Odyssey: From Main Sequence to Supernova*, 212, 91
- Gorda, S. Y. 2015, *Astronomy Letters*, 41, 276
- Grunhut, J. H., Wade, G. A., Leutenegger, M., et al. 2013, *MNRAS*, 428, 1686
- Grunhut, J. H., Wade, G. A., Neiner, C., et al. 2016, *MNRAS*, in press (arxiv: 1610.07895)
- Haefner, R., Simon, K. P., & Fiedler, A. 1994, *Information Bulletin on Variable Stars*, 3969, 1
- Harries, T. J., Hilditch, R. W., & Hill, G. 1997, *MNRAS*, 285, 277
- Harries, T. J., Hilditch, R. W., & Hill, G. 1998, *MNRAS*, 295, 386
- Howarth, I. D., Siebert, K. W., Hussain, G. A. J., & Prinja, R. K. 1997, *MNRAS*, 284, 265
- Hubrig, S., Schöller, M., Schnerr, R. S., et al. 2008, *A&A*, 490, 793
- Hubrig, S., Kholtygin, A., Scholler, M., et al. 2012, *Information Bulletin on Variable Stars*, 6019, 1
- Kochukhov, O., Makaganiuk, V., & Piskunov, N. 2010, *A&A*, 524, A5
- Kolenberg, K., & Bagnulo, S. 2009, *A&A*, 498, 543
- Kumsiashvili, M. I., Kochiashvili, N. T., & Djurasevi, G. 2005, *Astrophysics*, 48, 44
- Kupka, F., Piskunov, N., Ryabchikova, T. A., Stempels, H. C., & Weiss, W. W. 1999, *A&AS*, 138, 119
- Langer, N. 2014, *Magnetic Fields throughout Stellar Evolution*, 302, 1
- Li, Y.-F., & Leung, K.-C. 1985, *ApJ*, 298, 345
- Linder, N., Rauw, G., Pollock, A. M. T., & Stevens, I. R. 2006, *MNRAS*, 370, 1623
- Linder, N., Rauw, G., Sana, H., De Becker, M., & Gosset, E. 2007, *A&A*, 474, 193
- Linder, N., 2008, PhD thesis, Univ. of Liège
- Linder, N., Rauw, G., Martins, F., et al. 2008, *A&A*, 489, 713
- Lorenz, R., Mayer, P., & Drechsel, H. 1998, *A&A*, 332, 909
- Lorenz, R., Mayer, P., & Drechsel, H. 1994, *A&A*, 291, 185
- McSwain, M. V., & Gies, D. R. 2005, *ApJS*, 161, 118
- Mahy, L., Martins, F., Machado, C., Donati, J.-F., & Bouret, J.-C. 2011, *A&A*, 533, A9
- Martins, F., Donati, J.-F., Marcolino, W. L. F., et al. 2010, *MNRAS*, 407, 1423
- Mathys, G. 1989, *Fundamentals Cosmic Phys.*, 13, 143
- Mayer, P., Lorenz, R., & Drechsel, H. 2002, *A&A*, 388, 268
- Mayer, P., Harmanec, P., Nesslinger, S., et al. 2008, *A&A*, 481, 183
- Mayer, P., Drechsel, H., Harmanec, P., Yang, S., & Šlechta, M. 2013, *A&A*, 559, A22
- Moss, D. 2001, *Magnetic Fields Across the Hertzsprung-Russell Diagram*, 248, 305
- Nazé, Y., Bagnulo, S., Petit, V., et al. 2012, *MNRAS*, 423, 3413
- Neiner, C., Grunhut, J., Leroy, B., De Becker, M., & Rauw, G. 2015a, *A&A*, 575, A66
- Neiner, C., Mathis, S., Alecian, E., et al. 2015b, *Polarimetry, proc. of IAU symposium #305*, 61
- Niemela, V. S., Cerruti, M. A., Morrell, N. I., & Luna, H. G. 1992, *Evolutionary Processes in Interacting Binary Stars*, 151, 505
- Özdemir, S., Mayer, P., Drechsel, H., Demircan, O., & Ak, H. 2003, *A&A*, 403, 675
- Palate, M., Rauw, G., Koenigsberger, G., & Moreno, E. 2013, *A&A*, 552, A39
- Palate, M., Rauw, G., & Mahy, L. 2013, *Central European Astrophysical Bulletin*, 37, 311
- Palate, M., & Rauw, G. 2014, *A&A*, 572, A16
- Penny, L. R., Gies, D. R., Wise, J. H., Stickland, D. J., & Lloyd, C. 2002, *ApJ*, 575, 1050
- Penny, L. R., Ouzts, C., & Gies, D. R. 2008, *ApJ*, 681, 554
- Petit, V., & Wade, G. A. 2012, *MNRAS*, 420, 773
- Petit, V., Owocki, S. P., Wade, G. A., et al. 2013, *MNRAS*, 429, 398
- Piskunov, N. E., Kupka, F., Ryabchikova, T. A., Weiss, W. W., & Jeffery, C. S. 1995, *A&AS*, 112, 525
- Plaskett, J. S. 1922, *J. R. Astron. Soc. Canada*, 16, 284
- Qian, S.-B., Yuan, J.-Z., Liu, L., et al. 2007, *MNRAS*, 380, 1599
- Rauw, G., Nazé, Y., Carrier, F., et al. 2001, *A&A*, 368, 212
- Raucq, F., Rauw, G., Gosset, E., et al. 2016, *A&A*, 588, A10
- Rivinius, T., Carciofi, A. C., & Martayan, C. 2013, *A&ARv*, 21, 69
- Sana, H., Rauw, G., & Gosset, E. 2001, *A&A*, 370, 121
- Sana, H., Stevens, I. R., Gosset, E., Rauw, G., & Vreux, J.-M. 2004, *MNRAS*, 350, 809
- Schneider, F. R. N., Podsiadlowski, P., Langer, N., Castro, N., & Fossati, L. 2016, *MNRAS*, 457, 2355
- Spruit, H. C. 2002, *A&A*, 381, 923
- Stahl, O., Kaufer, A., Rivinius, T., et al. 1996, *A&A*, 312, 539
- Stickland, D. J., Koch, R. H., Pachoulakis, I., & Pfeiffer, R. J. 1994, *The Observatory*, 114, 107
- Stickland, D. J. 1997, *The Observatory*, 117, 37
- Szeifert, T., Appenzeller, I., Fuertig, W., et al. 1998, *Proc. SPIE*, 3355, 20
- Tamajo, E., Munari, U., Siviero, A., Tomasella, L., & Dallaporta, S. 2012, *A&A*, 539, A139
- Tout, C. A., Wickramasinghe, D. T., Liebert, J., Ferrario, L., & Pringle, J. E. 2008, *MNRAS*, 387, 897
- Thaller, M. L., Gies, D. R., Fullerton, A. W., Kaper, L., & Wiemker, R. 2001, *ApJ*, 554, 1070
- van Bever, J., & Vanbeveren, D. 1997, *A&A*, 322, 116
- Wade, G. A., Howarth, I. D., Townsend, R. H. D., et al. 2011, *MNRAS*, 416, 3160
- Wade, G. A., Grunhut, J., Gräfener, G., et al. 2012a, *MNRAS*, 419, 2459
- Wade, G. A., Maíz Apellániz, J., Martins, F., et al. 2012b, *MNRAS*, 425, 1278
- Wade, G. A., Barbá, R. H., Grunhut, J., et al. 2015, *MNRAS*, 447, 2551
- Wade, G. A., Neiner, C., Alecian, E., et al. 2016a, *MNRAS*, 456, 2
- Wade, G. A., Petit, V., Grunhut, J. H., Neiner, C., & MiMeS Collaboration 2016b, *Bright Emissaries: Be Stars as Messengers of Star-Disk Physics*, 506, 207
- Wickramasinghe, D. T., Tout, C. A., & Ferrario, L. 2014, *MNRAS*, 437, 675
- Yaşarsoy, B., & Yakut, K. 2013, *AJ*, 145, 9
- Zhao, E., Qian, S., Li, L., et al. 2014, *New Astron.*, 26, 112

This paper has been typeset from a $\text{\TeX}/\text{\LaTeX}$ file prepared by the author.